Available online at www.sciencedirect.com
SCIENCE DIRECT
Catalysis Today 102–103 (2005) 234–241
CATALYSIS TODAY
www.elsevier.com/locate/cattod

Hydrodechlorination of 1,2-dichloroethane on Pd–Ag catalysts supported on tailored texture carbon xerogels

Nathalie Job [a], Benoit Heinrichs [a,*], Fabrice Ferauche [a], Francis Noville [a], José Marien [b], Jean-Paul Pirard [a]

[a] *Laboratoire de Génie Chimique, B6a, Université de Liège, B-4000 Liège, Belgium*
[b] *Laboratoire de Physicochimie des Surfaces, B6c, Université de Liège, B-4000 Liège, Belgium*

Available online 24 March 2005

Abstract

Porous carbon xerogels synthesized in a previous study were investigated as catalysts supports. The support chosen was a micro-mesoporous carbon xerogel obtained from the pyrolysis of a resorcinol–formaldehyde resin whose synthesis variables were fixed at suitable values. Palladium and silver were deposited on this tailored texture carbon by co-impregnation using a solution of palladium and silver nitrates in nitric acid and water. Several catalysts were prepared with various Pd and Ag global contents, the latters being measured experimentally. Alloy particles, detected in all bimetallic samples, were studied by a combination of various techniques that enabled us to obtain their size as well as their bulk and surface composition. When present, the fraction of unalloyed silver was also calculated. The characterization data were related to the results of catalytic tests obtained for selective hydrodechlorination of 1,2-dichloroethane into ethylene. Results show that when the Ag content is too high, pure Ag particles are formed and the alloy composition remains constant. As a consequence, the surface composition of the alloy is constant as well and the catalytic tests lead to similar results.

Keywords: Hydrodechlorination; Carbon xerogels; Tailored texture carbon; 1,2-Dichloroethane

1. Introduction

Carbon porous materials with controlled texture can be synthesized by evaporative drying and pyrolysis of aqueous resorcinol–formaldehyde gels provided that the operating variables are correctly chosen [1–3]. The pore texture of those materials is mainly tailored by the pH of the precursors solution. Gels synthesized with pH values between 5.50 and 6.25 lead to micro-mesoporous carbon materials whose pore volume and maximum pore size increase when the synthesis pH decreases [3]. When the pH is lower than 5.50, the carbon is micro- and macroporous and looses its mechanical properties. When the pH exceeds 6.25, the material obtained is totally non porous. The ability to control their porous texture gives carbon xerogels an advantage with regard to active charcoals whose texture is mainly microporous and strongly depends on the selected raw material. The presence of mesopores should minimize diffusion limitations in catalysts carbon supports synthesized by sol–gel process, and these supports could be designed as desired depending on the considered reaction. In addition, these carbon materials possess a very good mechanical strength and monoliths of various shapes can be easily produced.

Carbon aerogels (i.e. dried by the supercritical method) were successfully used as catalysts supports [4]. Bimetallic Pd–Ag catalysts supported on active charcoals have been proved to be efficient for selective hydrodechlorination of chlorinated alkanes into alkenes [5]. One aim of the present study is to evaluate the potential of Pd–Ag alloys supported on synthetic carbon xerogels for such a reaction. Pd–Ag catalysts have been prepared by wet impregnation of a selected micro-mesoporous carbon xerogel with a solution containing nitric acid, water, $AgNO_3$ and $Pd(NO_3)_2{\cdot}2H_2O$. A series of five catalysts theoretically containing 1.5 wt.% Pd and various amounts of Ag (0–3 wt.%) was prepared. A pure Ag catalyst (1.5 wt.%) was also synthesized as a

* Corresponding author. Tel.: +32 4 366 35 05; fax: +32 4 366 35 45.
E-mail address: b.heinrichs@ulg.ac.be (B. Heinrichs).

0920-5861/$ – see front matter © 2005 Elsevier B.V. All rights reserved.
doi:10.1016/j.cattod.2005.02.021

reference. After drying, samples were reduced under H_2 flow at 350 °C in order to obtain metallic particles.

X-ray diffraction (XRD), transmission electron microscopy (TEM), CO chemisorption and inductively coupled plasma-mass spectroscopy (ICP-MS) analysis enabled us to determine the alloy particles size, the alloy global composition, the alloy surface composition and the actual metals weight percentages. The catalysts were tested for the selective hydrodechlorination of 1,2-dichloroethane into ethylene. Conversion and selectivities were related to the catalysts properties, in particular to the surface composition of the alloy particles in each Pd–Ag sample.

2. Experimental

2.1. Synthesis of carbon xerogel supported Pd–Ag catalysts

The synthesis process of carbon xerogels was extensively described elsewhere [3]. The selected support was obtained from evaporative drying and pyrolysis of an aqueous resorcinol–formaldehyde gel with a dilution ratio $D = 5.7$ (D = solvent/reactants molar ratio), a resorcinol/formaldehyde molar ratio $R/F = 0.5$, and an initial solution pH = 5.70. The aqueous gel obtained after gelation and ageing at 85 °C was then dried by vacuum evaporation without any pre-treatment. After drying, the gel was pyrolyzed at 800 °C under nitrogen flow in a tubular oven.

The pore texture of the carbon support obtained was determined by analysis of the nitrogen adsorption–desorption isotherms. The main texture parameters are: mesopore volume, $V_{meso} = 1.14$ cm^3/g; micropore volume, $V_{micro} = 0.25$ cm^3/g and $S_{BET} = 575$ m^2/g. No macropores were detected by mercury porosimetry.

The support was then crushed and sieved between 250×10^{-6} and 500×10^{-6} m. Five samples of the obtained pellets were impregnated with nitric acid solutions containing various amounts of $AgNO_3$ and $Pd(NO_3)_2{\cdot}2H_2O$. The metal concentrations of the various impregnating solutions were calculated so that the final Pd wt.% in all catalysts was theoretically maintained at 1.5% whereas Ag wt.% was chosen to be 0%, 0.75%, 1.5% or 3%. A pure Ag catalyst (1.5 wt.%) was also synthesized as a reference. Calculations of theoretical metal contents are based upon two hypothesis: (i) the concentration of the solution in excess after impregnation (eliminated by filtration) is identical to the one of the initial solution; (ii) all the metal that entered the pores after impregnation remains trapped after drying. The actual catalyst composition might of course differ from the theoretical composition.

Five $AgNO_3$ aqueous solutions with various concentrations were first prepared. Five millilitres from a solution containing 0.926 g $Pd(NO_3)_2{\cdot}H_2O$ in 25 ml aqueous nitric acid (69 wt.%) were added to 1.5 ml of each $AgNO_3$ solution. In the case of monometallic samples, one of the metal salt solutions was replaced by its pure solvent. The final composition of the impregnating solutions is reported in Table 1.

Carbon pellets (2 g) were immersed in 4 ml of each solution for 24 h. The samples were then filtered in order to remove the excess of solution and dried under flowing air (ambient temperature) for 24 h. The drying process was completed by vacuum drying (24 h, 150 °C). After drying, the samples to be characterized were reduced in flowing H_2 (H_2 flowrate: 0.025 mmol s^{-1} from room temperature, heating rate: 350 K h^{-1}, final temperature: 623 K, duration: 3 h).

From catalysts nominal metal contents the theoretical atomic ratio $[Pd/(Pd + Ag)]_{th}$ was calculated and the nomenclature of the five samples is related to this variable (Table 1).

2.2. Sample characterization

The pore texture of pure carbon xerogel as well as Pd/C, Ag/C and Pd–Ag/C catalysts was characterized by the analysis of nitrogen adsorption–desorption isotherms performed at 77 K with a sorptomatic Carlo Erba 1900 instrument.

Actual metal contents were determined from inductively coupled plasma-mass spectroscopy. The instrument was a VG Elemental Plasma Quad PQ2. Crushed sample (25 mg) were first digested in 5 ml fuming nitric acid and heated on a hot plate to incipient dryness. Deionised water (500 ml) was then added, and 5 ml of this solution were diluted with 0.75 ml of an internal standard ($^{115}In + {}^{187}Re + {}^{209}Bi$, 50 ng/l) and 19.25 ml water [6].

Metal particles were examined by XRD, TEM and CO chemisorption.

The XRD patterns were obtained with hand-pressed samples mounted on a Siemens D5000 goniometer using the Cu Kα line (Ni filter).

Table 1
Impregnation solution compositions and metal nominal contents

Catalyst	Solution composition				Metal nominal content		
	HNO_3 (69 wt.%) (ml)	H_2O (ml)	$Pd(NO_3)_2{\cdot}H_2O$ (g)	$AgNO_3$ (g)	Pd (wt.%)	Ag (wt.%)	$[Pd/(Pd + Ag)]_{th}$ (at.%)
Pd–Ag (100–0)	5	1.5	0.1852	0	1.5	0	100
Pd–Ag (67–33)	5	1.5	0.1852	0.0673	1.5	0.75	67
Pd–Ag (50–50)	5	1.5	0.1852	0.1347	1.5	1.5	50
Pd–Ag (33–67)	5	1.5	0.1852	0.2694	1.5	3.0	33
Pd–Ag (0–100)	5	1.5	0	0.1347	0	1	0

Transmission electron micrographs were obtained with a Philips CM100 microscope. All samples were crushed and dispersed in ethanol before deposition on a copper grid.

A volumetric static method was used for CO chemisorption [7]. Measurements were obtained on a Fisons sorptomatic 1990 equipped with turbomolecular vacuum pump which allows to reach a high vacuum of 10^{-6} kPa. The sample preparation and measurement method can be found in a previous study [8]. Carbon monoxide adsorption was performed at 303 K. As both chemisorption (on the Pd surface atoms) and physisorption (on metallic sites and support surface) occur at the catalyst surface, it is necessary to separate chemisorption and physisorption effects. A first CO adsorption isotherm was achieved so as to measure the total amount of adsorbed carbon monoxide (chemisorbed + physisorbed). The catalyst was then outgassed on the measurement unit at 303 K for 2 h in a vacuum of 10^{-6} kPa, and a second CO adsorption isotherm was measured in order to evaluate the amount of physisorbed CO. The total CO chemisorbed amount was deduced by subtracting the second isotherm from the first one and extrapolating the nearly horizontal difference curve to the uptake axis.

2.3. Catalytic tests

The catalysts were tested for selective hydrodechlorination of 1,2-dichloroethane into ethylene. It was decided to operate the reactor at low conversion. The feeding section of the kinetic measurement device was constituted of two gas lines for H_2 and He whose flowrates were adjusted with Brooks mass flowrate controllers. 1,2-Dichloroethane was supplied in liquid phase with a Gilson piston pump. A loop located in the oven upstream from the reactor ensured the vaporization of CH_2Cl–CH_2Cl.

The stainless steel tubular reactor with an internal diameter of 5×10^{-3} m and a length of 0.2 m was placed in a convection oven whose temperature was controlled and programmed. The temperature within the reactor was measured with a thermocouple slipped in a stainless steel sheath immersed in the catalyst bed. The total pressure was maintained constant *via* a pressure controller operating a compressed air valve located downstream from the reactor. For all kinetic measurements, the total pressure was fixed at 0.3 MPa. Feed gases flows were maintained constant *via* mass flow controllers: 37 Nl h^{-1} (0.459 mmol s^{-1}) helium and 2 Nl h^{-1} (0.025 mmol s^{-1}) hydrogen. The dichloroethane flow was equal to 1 Nl h^{-1} (0.012 mmol s^{-1}). The temperature within the reactor was fixed successively at 473, 523, 573 and 623 K.

The effluent of the reactor was analyzed by gas chromatography with a flame ionization detector (FID). Although this analysis method theoretically enabled us to measure 1,2-dichloroethane, ethylene and ethane concentrations, only C_2H_4 and C_2H_6 concentrations will be used in this study due to the too large imprecision of CH_2Cl–CH_2Cl concentration measurements.

The 9.4×10^{-3} m high catalytic bed is constituted of 0.75×10^{-3} kg of non reduced Pd/C or Pd–Ag/C catalyst pellets (250×10^{-6} and 500×10^{-6} m in diameter). Prior to the measurement, the catalyst was reduced in situ according to the following procedure: under flowing hydrogen (2 Nl h^{-1} = 0.025 mmol s^{-1}) and at a pressure of 0.125 MPa, the catalyst is heated from room temperature to 623 K at a rate of 350 K h^{-1} and is maintained at 623 K for 3 h. The reaction conditions were chosen so as to eliminate all external diffusion limitations. The absence of internal diffusion limitations was demonstrated by calculation as well as experimentally [9].

3. Results

3.1. Catalysts characterization

The nitrogen adsorption–desorption isotherms corresponding to the support alone and to the final catalysts after impregnation, drying and reduction treatments are quite identical. This shows that no modification of the carbon texture occurs during the metal deposition process.

Table 2 regroups results obtained from ICP, XRD, TEM and CO chemisorption.

The actual palladium content Pd_{ICP} (1.4–1.6 wt.%) is, in each sample, close to the nominal value (1.5 wt.%). The actual silver content Ag_{ICP} deviates from expected values. Nevertheless, the atomic ratio $[Pd/(Pd + Ag)]_{ICP}$ remains close to its theoretical value $[Pd/(Pd + Ag)]_{th}$ (Table 1).

Fig. 1 shows the diffractograms obtained for the five samples. The (1 1 1) Bragg lines of pure Pd ($2\theta = 40.114$) and pure Ag ($2\theta = 38.116$) are represented by the grey vertical lines. Between these two extremes, the bimetallic samples exhibit a broad peak which indicates the presence of small alloy particles. The three vertical black lines correspond to the maxima of these diffraction peaks after spectra deconvolution. The fraction of Pd atoms in the bulk of the alloy particles, x_{Pd} (Table 2), can be deduced from the alloy peak position [10]. Assuming that, in one given sample, all the bimetallic particles have the same Pd–Ag composition, their mean size (d_{XRD}) can be calculated from the peak broadening and Scherrer's formula [11]. Note that the particles composition may, in fact, vary to some extent, and that the results obtained from XRD are mean results for each bimetallic catalyst.

As the Ag content increases in the catalyst, the peak corresponding to the Pd–Ag alloy particles is shifted to smaller angles, which suggests an alloy enrichment in Ag. Nevertheless Pd–Ag (50–50) and Pd–Ag (33–67) exhibit alloy compositions that are not significantly different within the experimental error (49 and 53 at.% of Pd, respectively). The size of the alloy particles, d_{XRD}, is almost constant (3.6–4.3 nm) whereas pure Pd and pure Ag samples display particles size equal to 3.6 and 8.7 nm, respectively. Moreover, in samples Pd–Ag (50–50) and Pd–Ag (33–

Table 2
Results from ICP, XRD, TEM and CO chemisorption

Catalyst	ICP			XRD			TEM							CO
	Pd_{ICP} (wt.%)	Ag_{ICP} (wt.%)	$[Pd/(Pd+Ag)]_{ICP}$ (at.%)	x_{Pd} (at.%)	d_{XRD} (nm)	$d_{Ag\text{-}XRD}$ (nm)	d_{TEM1} (nm)	σ_1 (nm)	d_{TEM2} (nm)	σ_2 (nm)	d_{s1} (nm)	d_{v1} (nm)	d_{v2} (nm)	$n_{s,m}$ (mmol/g_{Pd})
Pd–Ag (100–0)	1.4	0	100	100	3.6	–[a]	3.1	0.8	–[a]	–[a]	–[b]	3.7	–[a]	1.62
Pd–Ag (67–33)	1.6	0.9	64	64	3.7	–[a]	3.0	0.9	–[a]	–[a]	3.5	3.7	–[a]	0.77
Pd–Ag (50–50)	1.6	1.9	46	49	4.1	–[c]	3.5	1.2	8.3	1.5	4.5	4.7	8.7	0.45
Pd–Ag (33–67)	1.5	2.4	38	53	4.3	9.2	3.0	0.7	7.9	1.2	3.9	4.1	9.4	0.62
Pd–Ag (0–100)	0	1.7	0	0	–[a]	8.7	7.9	2.5	–[a]	–[a]	–[b]	10.8	–[a]	–[a]

Pd_{ICP}, Ag_{ICP}: Pd and Ag contents in the catalyst measured by ICP-MS; x_{Pd}: fraction of Pd atoms in the bulk of Pd–Ag alloy particles estimated from XRD; d_{XRD}: mean size of Pd–Ag particles estimated from X-ray line broadening; d_{Ag-XRD}: mean size of pure Ag particles estimated from X-ray line broadening; d_{TEM1}, d_{TEM2}: mean particles sizes estimated from TEM for the two families of particles; σ_1, σ_2: standard deviations associated with d_{TEM1} and d_{TEM2}, respectively; d_{s1}: mean surface diameter of Pd–Ag alloy particles, $\sum n_i d_i^3 / n_i d_i^2$, estimated from TEM; d_{v1}, d_{v2}: mean volume diameter of metal particles, $\sum n_i d_i^4 / n_i d_i^3$, estimated from TEM for the two families of particles; $n_{s,m}$: amount of CO needed to form a chemisorbed monolayer on surface Pd atoms.

[a] Meaningless.
[b] Calculated for bimetallic samples only.
[c] Not measurable.

67), pure silver particles are detected by the presence of a shoulder whose position corresponds to the (1 1 1) Bragg line of Ag. That shoulder is hardly distinguishable on raw spectra (Fig. 1), but it appears more clearly after spectra deconvolution. When possible, the Ag particles size ($d_{Ag\text{-}XRD}$) was calculated from the deconvoluted curves. The intensity of the shoulder is unfortunately too low in the case of Pd–Ag (50–50). In the case of Pd–Ag (33–67), $d_{Ag\text{-}XRD}$ is 9.2 nm, which is very similar to the particles size of pure Ag catalyst (8.7 nm). Nevertheless, as the intensity of this peak is very low, this measurement must be considered with carefulness.

Transmission electron microscopy enabled us to measure the metal particles size. Fifty to 70 particles were measured for each sample so that the data set was statistically significant. The particle size distribution was found to be monomodal for Pd–Ag (100–0) and Pd–Ag (67–33) with mean values, d_{TEM1}, of 3.1 and 3.0 nm, respectively (Fig. 2 and Table 2). No particles bigger than 5 nm are observed, and the particle size distribution is rather narrow (standard deviation, σ_1 = 0.8–0.9 nm). The pure Ag sample Pd–Ag (0–100) displays a monomodal particle size distribution as well, but the particles are generally bigger and the distribution is wider (diameters ranging from 4 to 20 nm; standard deviation, σ_1 = 2.5 nm). In the case of samples Pd–Ag (50–50) and Pd–Ag (33–67), the particles size distribution is bimodal (Fig. 2). The data were analysed by separating the two particles families. The mean particle diameters, d_{TEM1} and d_{TEM2}, and their respective standard deviations, σ_1 and σ_2, were calculated from a set of at least 30 particles for each particles family. In those two samples, d_{TEM1} and σ_1 are very similar to the values found for Pd–Ag (100–0) and Pd–Ag (67–33). d_{TEM2} and σ_2 are closer to the values of d_{TEM1} and σ_1 found for the pure silver sample.

Since CO chemisorption occurs on palladium only [8,12] and Pd content given by ICP-MS differs from one catalyst to another, the amount of chemisorbed CO, which corresponds to a monolayer of carbon monoxide adsorbed on the palladium surface, is given in Table 2 per g of Pd, $n_{s,m}$ (mmol g_{Pd}^{-1}). $n_{s,m}$ values, which are much lower in bimetallic catalysts than in pure Pd catalyst, will be used below to calculate the surface composition of Pd–Ag alloy particles.

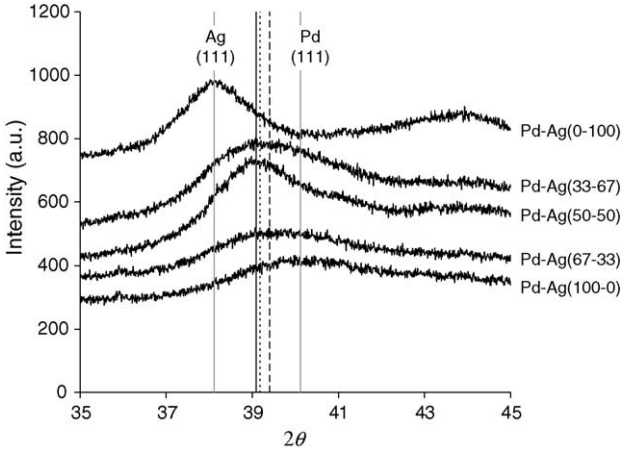

Fig. 1. X-ray diffractograms for the five catalysts. Peak maximum for the alloys: (- - -) Pd–Ag (67–33), (—) Pd–Ag (50–50), (. . .) Pd–Ag (33–67). The (1 1 1) Bragg lines of pure Pd and pure Ag appear in grey.

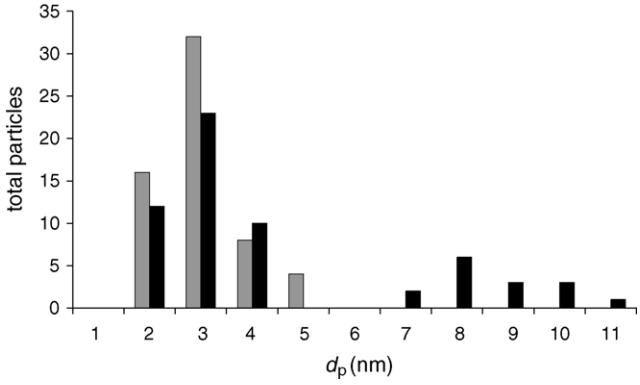

Fig. 2. Particles size distribution derived from the size measurement of 60 particles randomly chosen in each catalyst. (▒) Pd–Ag (67–33); (■) Pd–Ag (33–67).

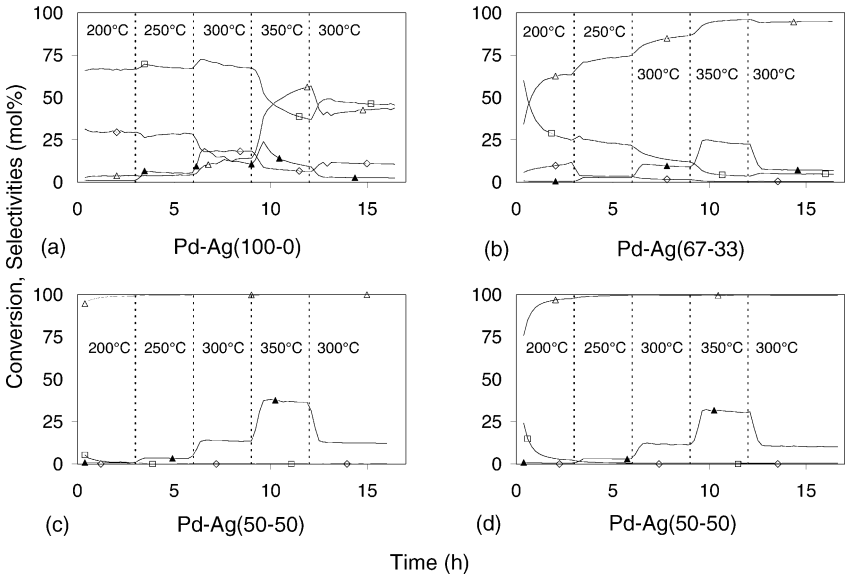

Fig. 3. Hydrodechlorination of 1,2-dichloroethane into ethylene: (▲) conversion; (△) ethylene selectivity; (□) ethane selectivity; (◇) chloroethane selectivity.

3.2. Catalytic tests

The results of the catalytic tests are presented in Fig. 3. Catalysts Pd–Ag (100–0), Pd–Ag (67–33), Pd–Ag (50–50) and Pd–Ag (33–67) convert CH_2Cl–CH_2Cl with an increasing selectivity in ethylene. At low temperature, the pure palladium sample Pd–Ag (100–0) (Fig. 3a) mainly produces ethane with a selectivity of about 70%. Chloroethane, which is not observed with the other catalysts (except small amounts with Pd–Ag (67–33) at low temperatures), is the main secondary product. When the temperature increases, ethylene selectivity increases markedly up to around 50% at 350 °C. By going down again to 300 °C at the end of the test, the final selectivities are as follows: about 45% for C_2H_4 and C_2H_6 and about 10% for CH_3–CH_2Cl. A deactivation is observed at all temperatures which is particularly strong at 350 °C. The introduction of silver into the catalyst leads to a drastic increase in C_2H_4 selectivity, and when the Ag loading is high enough, this selectivity reaches 100% at all temperatures. All the catalytic tests show that ethylene selectivity increases not only with temperature, but also with time, which indicates a temporal evolution of the catalyst due to its contact with the reacting atmosphere. Although a slight deactivation is still observed with all bimetallic catalysts, a comparison with the pure Pd sample Pd–Ag (100–0) shows that the introduction of silver stabilizes the catalyst.

4. Discussion

To make a comparison between the particle sizes obtained by XRD and TEM, it is necessary to remind that since XRD is sensitive to the volume of particles, the mean crystallite size calculated from the peak broadening corresponds to a volume weighted average diameter $\sum n_i d_i^4 / n_i d_i^3$ [11]. The mean volume diameter $d_v = \sum n_i d_i^4 / n_i d_i^3$ was then calculated from TEM micrographs. As some samples were found to display a bimodal particle size distribution, two distinct values of d_v (d_{v1} and d_{v2}), corresponding to the mean volume diameters of each particle groups, were calculated (Table 2). In the case of monomodal particle size distribution, d_{v2} is of course meaningless.

Regarding Pd–Ag (100–0) and Pd–Ag (67–33), the mean volume diameter d_{v1} is in each case similar to the Pd or alloy particles diameter evaluated by XRD, d_{XRD}. For Pd–Ag (0–100), the particle diameter obtained by XRD analysis ($d_{Ag\text{-}XRD}$ = 8.7 nm) is close to d_{v1} (10.8 nm). In the case of Pd–Ag (50–50) and Pd–Ag (33–67), the particle size distribution is bimodal and the mean volume diameters, d_{v1} and d_{v2}, of the two particle families can be compared to those of Pd–Ag alloy and pure Ag particles obtained from XRD. Indeed, in both samples, d_{v1} (4.7 and 4.1 nm, respectively) is very close to d_{XRD} (4.1 and 4.3 nm). d_{v2} is always larger (8.7–9.4 nm) and close to the size of pure silver particles in samples Pd–Ag (33–67) obtained by XRD ($d_{Ag\text{-}XRD}$ = 9.2 nm) and in sample Pd–Ag (0–100) obtained by XRD ($d_{Ag\text{-}XRD}$ = 8.7 nm) and by TEM (d_{v1} = 10.8 nm). These results suggest that, in the case of bimetallic catalysts, the Pd–Ag alloy tends to form a family of small particles (3–4 nm in diameter). When the Ag content increases, pure Ag particles whose diameter inclines to be larger (8–9 nm) are formed. Their amount increases slightly while the actual silver content Ag_{ICP} increases from 1.9% to 2.4%. Indeed, the composition of the alloy remains almost unchanged (the Ag atomic ratio of the alloy seems to be experimentally limited to about 50 at.%), and therefore, the extra quantities of silver are present in the catalyst in the form of pure silver particles.

Table 3
Fraction of alloyed Ag, Pd–Ag alloy dispersion, Pd dispersion and alloy surface composition

Catalyst	Ag_{alloy}/Ag_{total} (%)	D_{Pd-Ag} (%)	D_{Pd} (%)	x_{Pd_s} (at.%)
Pd–Ag (100–0)	–[a]	–[a]	25	100
Pd–Ag (67–33)	100	31	8	17
Pd–Ag (50–50)	89	24	5	10
Pd–Ag (33–67)	56	34	7	11

Ag_{alloy}/Ag_{total}: fraction of alloyed silver; D_{Pd-Ag}: overall dispersion of Pd–Ag alloy estimated from TEM; D_{Pd}: Pd dispersion estimated from CO chemisorption; x_{Pd_s}: fraction of Pd atoms present at the surface of Pd–Ag alloy particles estimated from the combination of CO chemisorption, XRD and TEM results.
[a] Meaningless.

The relative amount of alloyed silver, Ag_{alloy}/Ag_{total}, has been calculated in each bimetallic samples (Table 3). It decreases from 100% to 56% when the total Ag wt.% increases from 0.9% to 2.4% in the catalyst (Table 2). Note that the relative good agreement between the particle size measured by TEM ant the particle size derived from XRD results tends to indicate that the particles composition does not vary very much from one particle to another. If the composition was varying within the entire Pd–Ag composition interval, the XRD peak corresponding to the alloy would be much more broadened. The particle size would be underestimated compared to the actual size measured by TEM. On the contrary, the particles size measured by TEM is in each catalyst slightly smaller than the particles size obtained by XRD, due to the more pronounced influence of the biggest particles on the XRD signal.

The mean surface diameter of Pd–Ag alloy particles in bimetallic catalysts, $d_{s1} = \sum n_i d_i^3 / n_i d_i^2$, was also evaluated so that we could calculate the overall alloy dispersion, that is the ratio between the number of metal atoms at the surface of the Pd–Ag alloy particles and the total number of metal atoms in those particles, given by [11]:

$$D_{Pd-Ag} = \frac{6(v_m/a_m)}{d_{s1}} \quad (1)$$

where v_m is the mean volume occupied by a metal atom in the bulk of the alloy (nm^3) and a_m is the mean surface area occupied by a surface metal atom (nm^2). The values taken for v_m and a_m are arithmetic means of values given for Pd and Ag, that is $v_m = 0.01588\ nm^3$ and $a_m = 0.0834\ nm^2$ [11]. It must be specified that Eq. (1) is applied to alloy particles only. Pure silver particles that are detected in Pd–Ag (50–50) and Pd–Ag (33–67) are not taken into account. d_{s1} does then correspond to the mean surface diameter of the alloy particles only. Values obtained for D_{Pd-Ag} are listed in Table 3.

Since CO does not adsorb on silver particles [8,12], CO chemisorption provides a measurement of the palladium dispersion, and more specifically an estimation of the Pd content of the alloy surface. That content is higher in the bulk than on the alloy surface because of the lower surface energy of Ag in comparison with Pd [8]. In other words, the Pd–Ag alloy surface tends to get enriched in silver atoms. For bimetallic catalysts, the fraction of palladium atoms at the surface, x_{Pd_s}, can be deduced from a combination of CO chemisorption results with data coming from XRD and TEM [8]:

$$x_{Pd_s} = D_{Pd} x_{Pd} \frac{1}{D_{Pd-Ag}} \quad \text{with} \quad D_{Pd} = n_{s,m} M_{Pd} X_{Pd-CO} \times 10^{-3} \quad (2)$$

where x_{Pd_s} is the fraction of palladium atoms at the surface, D_{Pd} is the Pd dispersion (%) estimated from CO chemisorption, x_{Pd} is the fraction of Pd atoms in the bulk, D_{Pd-Ag} is the overall alloy dispersion with no distinction between the two metals, $n_{s,m}$ is the amount of CO needed to form a chemisorbed monolayer on palladium sites (mmol g_{Pd}^{-1}), M_{Pd} is the atomic weight of palladium (106.42 g mol^{-1}) and X_{Pd-CO} is the chemisorption mean stoichiometry, i.e. the mean number of Pd atoms on which one CO molecule is adsorbed. Soma-Noto and Satchler [12] demonstrated that $X_{Pd-CO} = 1$ (linear bonding) beyond 25 at.% of silver in the bulk of the alloy, which is the case for all the bimetallic samples examined here. In the case of CO chemisorption over Pd, it is well known that the chemisorption mean stoichiometry depends on the metal dispersion. Joyal and Butt [13] have determined the mean stoichiometry X_{Pd-CO} as a function of dispersion in Pd/SiO_2 catalysts and their results are used in an iterative method to calculate metal dispersion in Pd–Ag (100–0): (i) the starting value of 2 is used for X_{Pd-CO} and a first value of D_{Pd} is calculated from the CO monolayer uptake; (ii) by means of the table established by Joyal and Butt [13], a new value of X_{Pd-CO} is determined which corresponds to the precedent value obtained for D_{Pd}, and that new value of stoichiometry X_{Pd-CO} is used to calculate a new value of D_{Pd}. The cycle is repeated until convergence. In the case of pure Pd sample, this iterative calculation enabled us to obtain $X_{Pd-CO} = 1.45$ (combination of linear and multicenter bondings). Values of D_{Pd} and x_{Pd_s} are given in Table 3. A comparison between bulk (x_{Pd}) and surface (x_{Pd_s}) compositions confirms the surface enrichment with silver (Tables 2 and 3). As the bulk composition of the alloy is approximately identical in Pd–Ag (50–50) and Pd–Ag (33–67), the surface compositions are also identical.

Catalysts used for hydrodechlorination reactions are generally metals coming from group VIII [14–17]. The reaction mechanisms generally suggested imply a dissociative adsorption of the chlorinated alkane on the metal surface with successive breakings of C–Cl bonds. Further studies on chlorinated alkanes demonstrated the ability of bimetallic catalysts composed of one metal from group VIII and one from group Ib to transform chlorinated alkanes selectively into alkenes to the detriment of less useful alkanes [5,18–20]. In the case of Pd–Ag alloys, a previous study [21] showed that the reaction mechanism includes the following steps: (i) dissociative adsorption of 1,2-dichloroethane on Ag sites with successive breakings of the two C–Cl bonds

followed by (ii) desorption of ethylene and (iii) dechlorination of silver surface by hydrogen adsorbed on Pd (production of HCl). As Pd can store hydrogen by dissociative chemisorption, Pd present in the alloy supplies hydrogen atoms for the regeneration of the chlorinated Ag surface into metallic Ag. But hydrogen adsorbed on Pd may also cause undesired ethylene hydrogenation which is favoured by the presence of large amounts of Pd at the surface of the Pd–Ag alloy particles. Therefore, the selectivity of the Pd–Ag catalysts depends on the surface composition of the alloy.

Pure Pd catalyst Pd–Ag (100–0) is active but mainly produces ethane due to the ability of H_2 adsorbed on Pd to easily hydrogenate the double bond of ethylene adsorbed on the adjacent Pd atoms (Fig. 3a). When Ag is added to Pd in sufficient proportion (Fig. 3b), the catalyst mainly produces ethylene. In the case of Pd–Ag (67–33), the production of ethane cannot be avoided due to the relatively high amount of surface palladium atoms (17%). The ethane formation is almost totally eliminated when the total Ag content increases to 50 at.% (Pd–Ag (50–50), Fig. 3c): x_{Pd_s} decreases to 9.6%. In such a case, it has been shown that the Pd–Ag surface is constituted of Pd atoms isolated in the middle of silver atoms [22] and which are still able to chemisorb H_2 dissociatively [23].

Results obtained with Pd–Ag (33–67) are very similar, which was foreseeable since surface compositions of active Pd–Ag alloy nanoparticles in Pd–Ag (50–50) and in Pd–Ag (33–67) are identical within the experimental error. The only difference between these two catalysts is the amount of pure Ag particles present on the support, but as these particles are quickly saturated by chlorine, they do not influence the catalytic results.

5. Conclusion

Porous carbons with tailored texture can be obtained from evaporative drying and pyrolysis of resorcinol–formaldehyde aqueous gels whose synthesis variables are correctly chosen. Pd, Pd–Ag and Ag catalysts supported on micro-mesoporous carbon xerogels were successfully prepared by impregnation of such a support with nitric acid solutions containing palladium and silver nitrates in various proportions. The impregnation was followed by drying and metal reduction. The characterization techniques show that carbon xerogels are suitable supports to disperse finely catalytic metals. In the case of pure Pd catalyst, all metal particles are 2–5 nm in diameter. Small particles of silver are more difficult to obtain: the particle size distribution in the pure Ag catalyst is very wide (4–20 nm). In the case of bimetallic catalysts, an alloy is present at the surface of the support under the form of small particles (3–4 nm). The Ag content in the bulk alloy is nevertheless limited to about 50%: the extra quantities of Ag added to the impregnating solution are deposited on the carbon surface as pure Ag particles (6–15 nm). This limitation also fixes the minimum palladium surface content of the alloy at about 10%.

Catalytic tests show that Pd/C and Pd–Ag/C catalysts are active for the hydrodechlorination of 1,2-dichloroethane. As expected, pure Pd samples produce mainly ethane, whereas bimetallic catalysts are selective for the production of ethylene. The ethylene selectivity increases with the silver fraction at the alloy surface. As the surface composition is quasi identical for the samples whose silver global content exceeds 50 at.%, their catalytic performances are equivalent. These results are in good agreement with those found for similar catalysts prepared by other ways [5,24].

Acknowledgements

The authors thank the Belgian Fonds National de la Recherche Scientifique, the Région Wallonne—Direction Générale des Technologies, de la Recherche et de l'Energie, the Ministère de la Communauté française—Direction de la Recherche scientifique and the Fonds de Bay for their financial support. The authors are also grateful to J. Vander Auwera and G. Bologne from the Geology Department of the University of Liège for the ICP-MS measurements.

References

[1] J.-P. Pirard, R. Pirard, N. Job, European Patent Application EP1280215 (2003).
[2] N. Job, F. Ferauche, R. Pirard, J.-P. Pirard, Stud. Surf. Sci. Catal. 143 (2002) 619.
[3] N. Job, R. Pirard, J. Marien, J.-P. Pirard, Carbon 42 (2004) 619.
[4] G.M. Pajonk, A. Venkateswara Rao, N. Pinto, F. Ehrburger-Dolle, M. Bellido Gil, Stud. Surf. Sci. Catal. 118 (1998) 167.
[5] J.-P. Schoebrechts, F. Janssens, U.S. Patent 5 821 394 (1998).
[6] J. Vander Auwera, G. Bologne, I. Roelandts, J.-C. Duchesne, Geologica Belgica 1 (1998) 49–53.
[7] J.R. Anderson, Structure of Metallic Catalysts, Academic Press, London, 1975.
[8] B. Heinrichs, F. Noville, J.-P. Schoebrechts, J.-P. Pirard, J. Catal. 192 (2000) 108.
[9] F. Kapteijn, J.A. Moulijn, in: G. Ertl, H. Knözinger, J. Weitkamp (Eds.), Handbook of Heterogeneous Catalysis, vol. 3, Wiley-VCH, Weinheim, 1997, p. 1359.
[10] J.H. Sinfelt, Bimetallic Catalysts—Discoveries, Concepts, and Applications, Wiley, New York, 1983.
[11] G. Bergeret, P. Gallezot, in: G. Ertl, H. Knözinger, J. Weitkamp (Eds.), Handbook of Heterogeneous Catalysis, vol. 2, Wiley-VCH, Weinheim, 1997, p. 439.
[12] Y. Soma-Noto, W.M.H. Satchler, J. Catal. 32 (1974) 315.
[13] C.L.M. Joyal, J.B. Butt, J. Chem. Soc., Faraday Trans. 1 (83) (1987) 2757.
[14] S.C. Fung, J.H. Sinfelt, J. Catal. 103 (1987) 220.
[15] J.W. Bozzelli, Y.-M. Chen, S.S.C. Chuang, Chem. Eng. Commun. 115 (1992) 1.
[16] S. Lambert, C. Cellier, P. Grange, J.-P. Pirard, B. Heinrichs, J. Catal. 221 (2004) 335.
[17] S. Lambert, J.-F. Polard, J.-P. Pirard, B. Heinrichs, Appl. Catal. B 50 (2004) 127.
[18] L.N. Ito, A.D. Harley, M.T. Holbrook, D.D. Smith, C.B. Murchison, M.D. Cisneros, International Patent Application WO 94/07827 (1994).

[19] B. Heinrichs, P. Delhez, J.-P. Schoebrechts, J.-P. Pirard, J. Catal. 172 (1997) 322.
[20] L.S. Vadlamannati, V.I. Kovalchuk, J.L. d'Itri, Catal. Lett. 58 (1999) 173.
[21] B. Heinrichs, J.-P. Schoebrechts, J.-P. Pirard, J. Catal. 200 (2001) 308.
[22] G.A. Kok, A. Noordermeer, B.E. Nieuwenhuys, Surf. Sci. 152–153 (1985) 505.
[23] A. Noordermeer, G.A. Kok, B.E. Nieuwenhuys, Surf. Sci. 165 (1986) 375.
[24] P. Delhez, B. Heinrichs, J.-P. Pirard, J.-P. Schoebrechts, U.S. Patent 6 072 096 (2000).